The Astrophysical Journal Letters, 816:L22 (6pp), 2016 January 10 doi:10.3847/2041-8205/816/2/L22

EVIDENCE FOR GAS FROM A DISINTEGRATING EXTRASOLAR ASTEROID*

S. Xu (许偲艺)[1], M. Jura[2], P. Dufour[3], and B. Zuckerman[2]
[1] European Southern Observatory, Karl-Schwarzschild-Straße 2, D-85748 Garching, Germany; sxu@eso.org
[2] Department of Physics and Astronomy, University of California, Los Angeles CA 90095-1562, USA; jura@astro.ucla.edu, ben@astro.ucla.edu
[3] Institut de Recherche sur les Exoplanètes (iREx), Université de Montréal, Montréal, QC H3C 3J7, Canada; dufourpa@astro.umontreal.ca
Received 2015 October 29; accepted 2015 November 13; published 2016 January 12

ABSTRACT

We report high-resolution spectroscopic observations of WD 1145+017—a white dwarf that was recently found to be transitted by multiple asteroid-sized objects within its tidal radius. We discovered numerous circumstellar absorption lines with linewidths of $\sim$300 km s^{-1} from Mg, Ca, Ti, Cr, Mn, Fe, and Ni, possibly from several gas streams produced by collisions among the actively disintegrating objects. The atmosphere of WD 1145+017 is polluted with 11 heavy elements, including O, Mg, Al, Si, Ca, Ti, V:, Cr, Mn, Fe, and Ni. Evidently, we are witnessing the active disintegration and subsequent accretion of an extrasolar asteroid.

Key words: circumstellar matter – minor planets, asteroids: general – stars: abundances – stars: individual (WD 1145+017) – white dwarfs

Supporting material: data behind figure

1. INTRODUCTION

Recent studies show that planetary systems are widespread around white dwarfs. About 25%–50% of white dwarfs show "pollution" in their atmospheres, likely from accretion of planetesimals that were perturbed by planet(s) into the white dwarf's tidal radius (Zuckerman et al. 2003, 2010; Koester et al. 2014). High-resolution spectroscopic observations of these polluted white dwarfs typically reveal abundances similar to the observed compositions of solar system objects (Jura & Young 2014). The most heavily polluted white dwarfs often have an infrared excess from an orbiting dust disk (Kilic et al. 2006). Occasionally, circumstellar gaseous material is also detected, mostly via calcium infrared triplet emission (Gänsicke et al. 2006; Debes et al. 2012; Melis et al. 2012).

These systems can be dynamically active. The infrared flux of the dust disk around WD J0959–0200 dropped $\sim$30% within one year (Xu & Jura 2014). The gas disk around WD J1617+1620 was dissipated within a few years (Wilson et al. 2014). One model to explain these changes is the impact of an extrasolar asteroid onto a pre-existing dust disk (Jura 2008). However, the parent body has never been detected.

In this letter, we report Keck spectroscopic observations of a helium-dominated white dwarf WD 1145+017. This star was first discovered in the Hamburg/ESO survey (Friedrich et al. 2000). It caught our attention due to the strong infrared excess when comparing SDSS, UKIDSS, and *WISE* photometry. After performing the Keck observations, we subsequently learned that this star happened to be located in a K2 field, and it was observed to be transitted by multiple objects with periods between 4.5 and 5.0 hr (Croll et al. 2015; Vanderburg et al. 2015). The system is rapidly evolving and the transit data are interpreted as cometary-like outflows from fragments of a larger parent body. Here, we provide additional evidence in support of this model.

* The data presented herein were obtained at the W.M. Keck Observatory, which is operated as a scientific partnership among Caltech, the University of California, and NASA. The Observatory was made possible by the generous financial support of the W.M. Keck Foundation.

2. OBSERVATIONS AND DATA REDUCTION

2.1. HIRES

WD 1145+017 was observed with the High Resolution Echelle Spectrometer (HIRES; Vogt et al. 1994) on the Keck I telescope on 2015 April 11 (UT). The blue collimator was chosen with the C5 decker, which has a slit width of 1.″148 and a resolution of $\sim$40,000. Three consecutive 2400 s exposures of WD 1145+017 were taken. The flux standard Feige 34 was observed with the same setup.

Data reduction was performed by using both MAKEE and IRAF following Klein et al. (2010) and Xu et al. (2014). We used the spectrum of Feige 34 to calibrate the target spectrum and reconstruct the profiles of broad helium lines. The three separate spectra were combined with equal weights to produce the final spectrum, which has wavelength coverage from 3110 to 5950 Å. The signal-to-noise ratio (S/N) per pixel is typically over 25.

We identified $\sim$200 photospheric absorption lines from 15 different ions. About one-third of these lines also show broad ($\sim$300 km s^{-1}) circumstellar absorption features, as shown in Figures 1 and 2. All circumstellar lines arise from energy levels within 4.2 eV of the ground state (see Table 2).

2.2. ESI

On 2015 April 25 (UT), we observed WD 1145+017 with the Echellette Spectrograph and Imager (ESI; Sheinis et al. 2002) on the Keck II telescope. The narrowest possible slit width of 0.″3 was chosen, corresponding to a resolution of $\sim$13,700. WD 1145+017 was observed with two consecutive 1180 s exposures. Data reduction was performed using the MAKEE package. Each echelle order was continuum normalized in IRAF with a low-order polynomial. The ESI spectrum has a usable coverage from 4000 to 10100 Å with an S/N per pixel over 35. Some lines were only detected in the ESI data due to its wide spectral coverage. Unfortunately, about two-thirds of the photospheric lines lie shortward of 4000 Å, which is not accessible with ESI. For the spectral region that overlaps

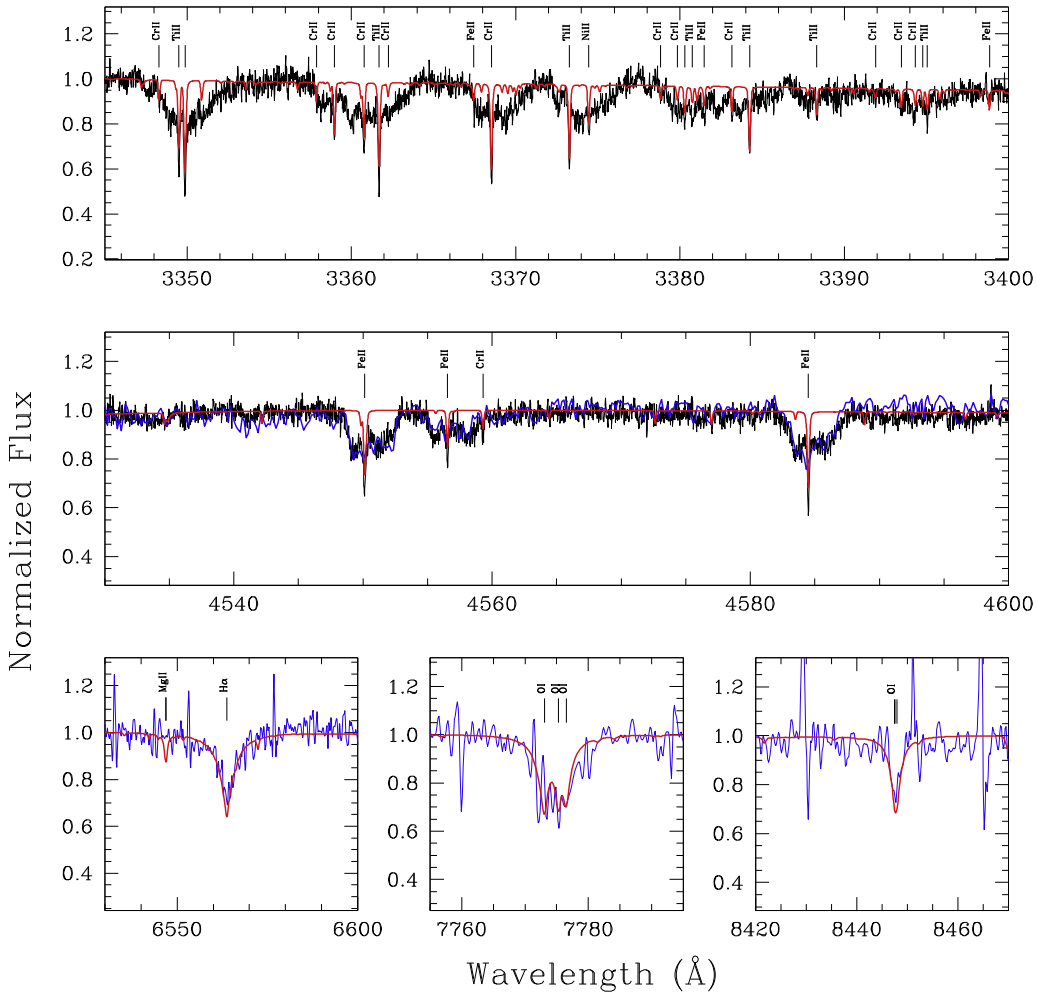

Figure 1. Portion of the Keck spectra. The black and blue lines represent the HIRES and ESI data, respectively, and the agreement is quite good for the middle panel. The red line is our best-fit model to the photospheric lines, presented in the heliocentric reference frame. Numerous photospheric and circumstellar lines are detected. The data used to create this figure are available.

with HIRES data (4000–5950 Å), the agreement is quite good, as shown in Figures 1 and 2.

3. DISCUSSION

3.1. Photospheric Abundances

We adopted an effective temperature of 15,900 K and a surface gravity of 8.0 for WD 1145+017 (Vanderburg et al. 2015). However, the surface gravity is highly uncertain because it cannot be derived unambiguously from spectroscopic fitting for helium white dwarfs below ∼16,500 K (Voss et al. 2007). To determine the abundances of heavy elements, we followed procedures outlined in Dufour et al. (2012) and fitted a spectral region of 10–15 Å at a time. HIRES data were used primarily for the analysis due to its higher spectral resolution. The final abundances and the photospheric lines are shown in Table 1.

Oxygen has lines only in the lower resolution ESI data. The best-fit model requires an oxygen abundance $\log n(\mathrm{O})/n(\mathrm{He})$ of −3.7 and −4.5 for the O I 7775 Å triplet and O I 8446 Å, respectively. The discrepancy cannot be due to contaminations from circumstellar absorption because the oxygen lines all arise from energy levels ∼9 eV above the ground state. A higher weight is given to O I 8446 Å because the O I triplet is not resolved, as shown in Figure 1.

The total mass of heavy elements currently in the outer convection zone of WD 1145+017 is 6.6×10^{23} g, about 70% the mass of Ceres. The planetesimal was dominated by four elements, O, Fe, Mg, and Si, similar to rocky objects in the solar system and extrasolar asteroids accreted onto other polluted white dwarfs, as shown in Figure 3 (e.g., Klein et al. 2010; Dufour et al. 2012; Jura & Young 2014). The mass fraction of oxygen is ∼60%, which is among the most oxygen-rich extrasolar planetesimals ever detected. However, due to the large error associated with the oxygen abundance, the oxygen abundance would be "normal" if it is at the lower end.

If the accretion is in a steady state (Koester 2009), the mass accretion rate for WD 1145+017 would be 4.3×10^{10} g s^{-1}, among the highest of all polluted white dwarfs. The accretion needs to be on-going for 5×10^5 years to accumulate a total mass of 6.6×10^{23} g. It is very unlikely that one tidal disruption event can last that long (Veras et al. 2015). In this case, the material currently in the white dwarf's photosphere would be associated with a previous tidal disruption event. Alternatively, WD 1145+017 could be in the very early stage of tidal disruption and it is experiencing a short high-accretion

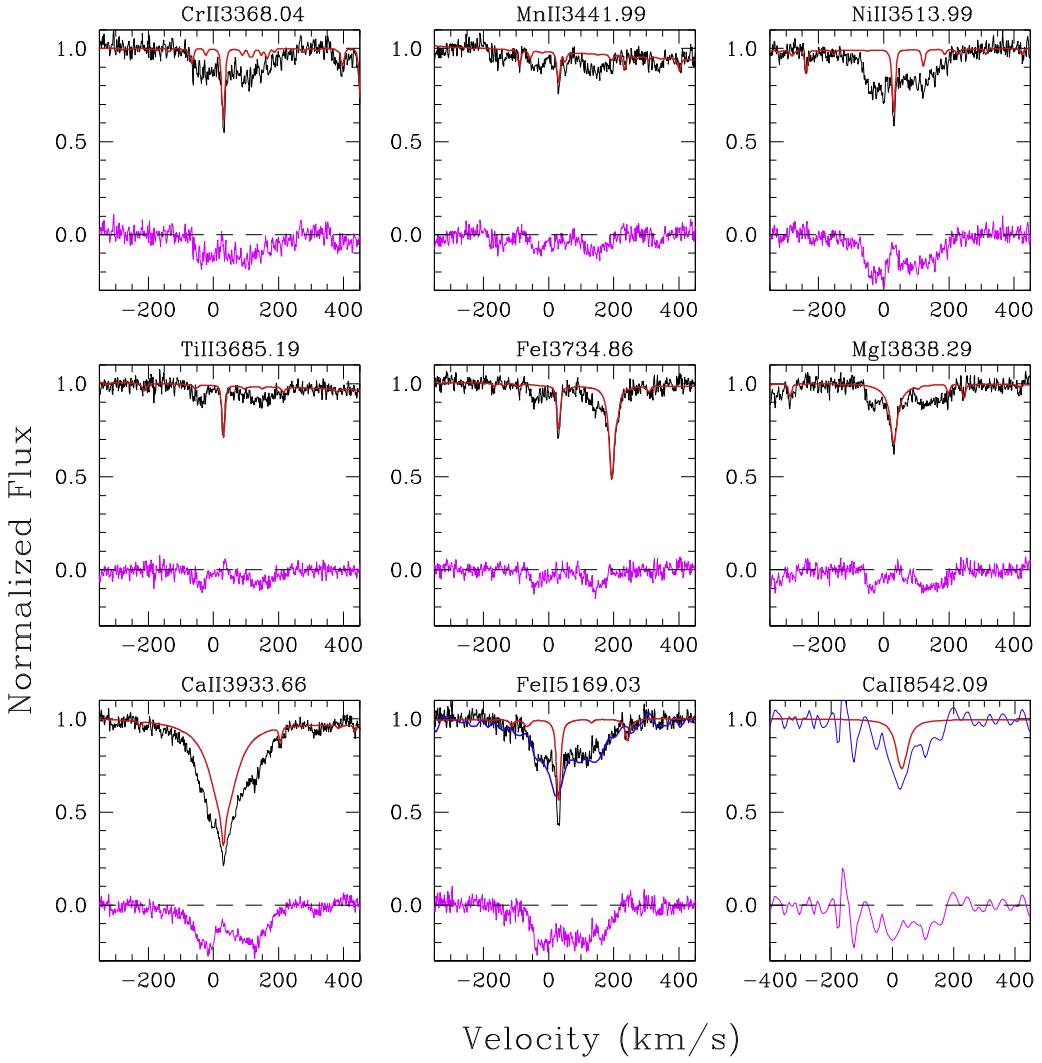

Figure 2. Similar to Figure 1, except in velocity space in the white dwarf's reference frame. The lower solid magenta line represents data minus photospheric model—there exists circumstellar absorption produced by gas between us and the white dwarf. All photospheric lines have a velocity of 30 km s^{-1} due to the gravitational redshift. The circumstellar lines are asymmetric and extend from −100 km s^{-1} to 210 km s^{-1}.

burst. Evidence for such bursts have been speculated in the literature but never been directly detected (Farihi et al. 2012; Xu & Jura 2014). The mass accretion rate can go up to 10^{13} g s^{-1}, approaching those of low accretion rate cataclysmic variables (Schmidt et al. 2007). In this scenario, the current tidal disruption event would have been on-going for 2000 years. The heavy elements in WD 1145+017 could also come from a combination of the two scenarios.

3.2. Circumstellar Gas

A large number of circumstellar absorption lines are detected, as shown in Figures 1 and 2. We observe relatively cool circumstellar gas blocking part of the white dwarf's photosphere. The line profiles are broad, asymmetric, and morphologically different from the narrow circumstellar features (that originate from ionization of the ISM) detected around hot white dwarfs (Holberg et al. 1995; Dickinson et al. 2012). They also differ from the symmetric blueshifted Si IV absorption lines detected around PG 0843+517, which is attributed to the presence of hot circumstellar gas (Gänsicke et al. 2012). Here, we present some qualitative analysis on the gas around WD 1145+017.

The gravitational redshift is estimated to be 30 km s^{-1} at the surface of WD 1145+017. In the heliocentric frame, the average radial velocity of the photospheric lines is 42 ± 2 km s^{-1}. We can derive the kinematic radial velocity of the white dwarf to be 12 km s^{-1}. In the reference frame of the white dwarf, the full velocity at zeroth intensity of the circumstellar absorption line extends from −100 to 210 km s^{-1} (see Figure 2). This broad line profile can be produced by several gas streams moving in non-circular motions and that likely are associated with the disintegrating planetesimals. Otherwise, if the gas motion is approximately circular, circumstellar absorption lines would be narrow with a radial velocity of ∼12 km s^{-1}—the kinematic radial velocity of the white dwarf.

As shown in Table 2, most circumstellar lines have an equivalent width around 0.5 Å, even though the abundances and oscillator strengths vary by more than three orders of magnitude; the implication is that most of the circumstellar lines are optically thick. However, the lines of the trace

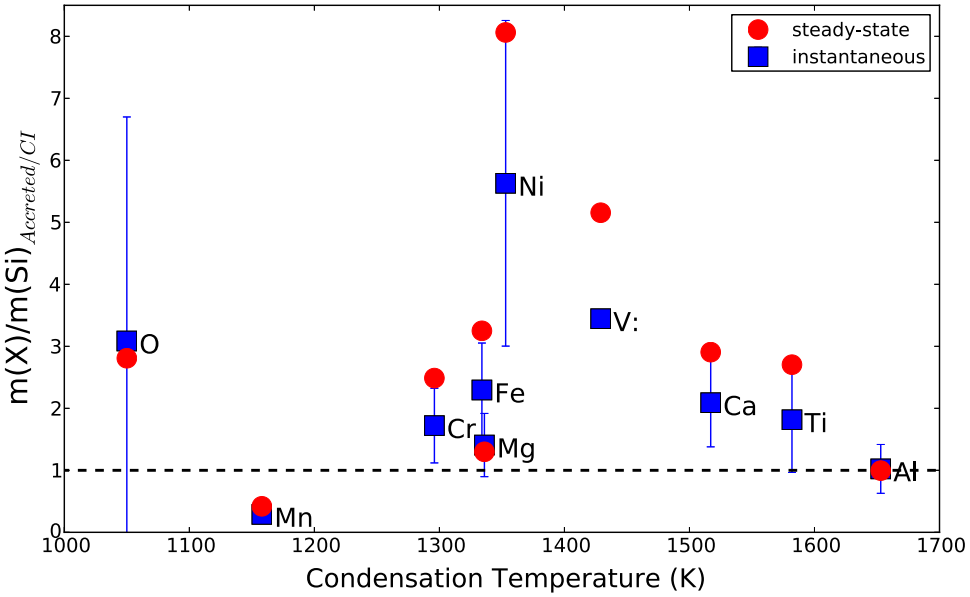

Figure 3. Mass fraction of an element relative to Si in the extrasolar material accreted onto WD 1145+017. The values are normalized to the ratios in CI chondrites (Wasson & Kallemeyn 1988). For example, a CI-chondrite analog would lie along the black dashed line. Two models are presented and the error bar is only shown for the instantaneous model (see Section 3.1). Within the uncertainties, the overall abundance pattern in the object accreted onto WD 1145+017 is similar to that in CI chondrites.

Table 1
Photospheric Absorption Lines and Abundance Determination

Ion	log n(Z)/n(He)	t^a (10^5 years)	M^b (10^{20} g)	$\dot{M}^c$ (10^8 g s^{-1})
H	-4.7 ± 0.1	...	...	...
C	<-4.3	6.0	<3200	<170
O	-4.3 ± 0.5	5.5	4300	240
Mg	-5.49 ± 0.13	5.5	410	24
Al	-6.74 ± 0.14	5.2	26	1.6
Si	-5.69 ± 0.09	5.0	300	19
Ca	-6.57 ± 0.12	3.6	58	5.1
Ti	-8.04 ± 0.19	3.4	2.3	0.22
V:	-8.7:	3.4	0.57	0.054
Cr	-7.31 ± 0.12	3.5	14	1.2
Mn	-8.25 ± 0.20	3.5	1.7	0.15
Fe	-5.35 ± 0.11	3.6	1300	120
Ni	-6.24 ± 0.18	3.5	180	16
Total	...	...	6600	430

Notes.
[a] Diffusion time out of the convection zone, following Dufour et al. (2012).
[b] Current mass in the white dwarf's convection zone.
[c] Accretion rate assuming a steady state (Koester 2009).
The following lines are free from circumstellar absorption and used for abundance determinations: H I 4861.3 Å, 6562.8 Å; C I 4267.3 Å; O I 7775 Å[de], 8446.4 Å[d]; Mg I 3829.4 Å, 5172.7 Å, 5183.6 Å; Mg II 4481.1 Å[e], 7877.1 Å[d], 7896.0 Å[d], 7896.4 Å[d]; Al II 3586.5 Å, 3587.0 Å, 3961.5 Å, 4663.1 Å; Si II 3853.7 Å, 3856.0 Å, 3862.6 Å, 4128.1 Å, 4130.9 Å, 5041.0 Å, 5056.0 Å, 6347.1 Å, 6371.4 Å; Ca II 3159.0 Å, 3181.4 Å, 3706.1 Å, 3737.0 Å, 8498.1 Å[d], 8542.2 Å[d]; Ti II 3239.0 Å, 3261.6 Å,3329.5 Å, 3504.9 Å; V II, 3271.1 Å; Cr II 3125.0 Å, 3180.7 Å, 3217.4 Å; Mn II, 3482.9 Å; Fe I, 3165.9 Å, 3565.4 Å, 3570.1 Å, 3606.7 Å, 3608.9 Å, 3618.8 Å, 3631.5 Å, 3719.9 Å, 3721.6 Å, 3749.5 Å, 3758.2 Å, 3815.8 Å,3820.4 Å, 3825.9 Å, 3859.9 Å, 4063.6 Å, 4071.7 Å, 4307.9 Å; Fe II, 3144.8 Å, 3177.5 Å, 3180.2 Å, 3183.1 Å, 3186.7 Å, 3237.8 Å, 3266.9 Å, 4635.3 Å, 4923.9 Å, 5260.3 Å, 6456.4 Å[d]; Ni I, 3524.5 Å; Ni II, 3374.0 Å, 3471.4 Å. ([d] This line is only detected in the ESI data and is given less weight when HIRES data for the same element are available. [e] This line is blended.)

constituent Mn might be optically thin because Mn II 3442.0 Å[4] and Mn II 3482.9 Å arise from the same lower energy level but have different equivalent widths, which are in proportion to their oscillator strengths. We calculated a Mn II column density of 4.7×10^{13} cm^{-2}. Assuming the circumstellar gas and the photosphere have the same elemental compositions, the Fe II column density N(Fe II) equals 3.7×10^{16} cm^{-2}, leading to opaque lines. We can also estimate the excitation temperature, which is ~a few thousand Kelvins. The heating mechanism might be similar to the Z II region model described in Melis et al. (2010).

As shown in Figure 2, all the circumstellar lines have about the same depth, indicating ~15% of the white dwarf's photosphere is covered by gas, which has a vertical thickness $h = 0.15 \times 2R_{\rm wd} = 2700$ km ($R_{\rm wd}$ from Vanderburg et al. 2015). If the radial distribution of the gas extends to the tidal radius (~100 $R_{\rm wd}$), the total mass of Fe II in the gas disk can be estimated as:

$$M\,({\rm Fe\ II}) = 2\pi \times 100R_{\rm wd} \times h \times N\,({\rm Fe\ II}) \times m\,({\rm Fe}) \quad (1)$$

where m(Fe) is the mass of one Fe atom. The total mass of Fe II gas is 1.0×10^{15} g. Assuming the mass fraction of Fe II is 25%, the total gas mass $M_{\rm gas}$ would be 4.2×10^{15} g.

If gas is being accreted at $V = 210$ km s^{-1}—the maximum observed radial velocity—we can derive a maximum accretion rate $\dot{M}$ as

$$\dot{M} = M_{\rm gas} \times \frac{V}{100R_{\rm wd}} = 1.0 \times 10^{12}\ {\rm g\ s^{-1}}. \quad (2)$$

This value is higher than the mass accretion rate onto the white dwarf's photosphere under the steady state assumption (4.3×10^{10} g s^{-1}). The accretion is likely to be a sporadic process. The gas lifetime can be calculated by dividing the total

[4] As shown in Figure 2, there is also a nearby Fe I line at 3442.3 Å. However, the Fe I line is unlikely to have circumstellar absorption due to its low oscillator strength ($f = 0.008$).

Table 2
Circumstellar Lines in WD 1145+017

Ion	λ[a] (Å)	E_{low} (eV)	f	EW[b] (Å)	N[c] (10^{12} cm^{-2})
Mg I	3832.3	2.7	0.45	0.05	>0.9
Mg I	3838.3	2.7	0.5	0.2	>3
Ca II[d]	3933.7	0.0	0.68	1.0	>11
Ca II[d]	3968.5	0.0	0.33	0.8	>17
Ca II[d]	8542.1	1.7	0.02	0.2	>18
Ti II	3341.9	0.6	0.38	0.3	>8
Ti II	3685.2	0.6	0.13	0.2	>10
Ti II	3761.3	0.6	0.26	0.1	>3
Ti II	3759.3	0.6	0.2	0.13	>5
Cr II	3403.3	2.4	0.043	0.2	>46
Cr II	3433.3	2.4	0.047	0.2	>43
Cr II	3125.0	2.5	0.31	0.5	>17
Cr II	3132.1	2.5	0.33	0.4	>15
Cr II	3368.1	2.5	0.10	0.3	>31
Cr II	3408.8	2.5	0.051	0.5	>96
Cr II	3422.7	2.5	0.064	0.3	>51
Mn II	3442.0	1.8	0.05	0.2	>46
Mn II	3482.9	1.8	0.029	<0.15	<48
Fe I	3581.2	0.9	0.23	0.1	>4.6
Fe I	3734.9	0.9	0.19	0.2	>8.6
Fe II	3281.3	1.0	0.0004	0.4	>9900
Fe II	3295.8	1.1	0.0003	0.4	>13000
Fe II	3227.7	1.7	0.018	0.7	>390
Fe II	4173.5	2.6	0.0012	0.2	>840
Fe II	4178.9	2.6	0.0006	0.2	>2000
Fe II	4233.2	2.6	0.0018	0.5	>1600
Fe II	4303.2	2.7	0.0006	0.2	>1900
Fe II	4351.8	2.7	0.0014	0.4	>1500
Fe II	4583.8	2.8	0.0012	0.6	>2700
Fe II	4629.3	2.8	0.0005	0.2	>2700
Fe II	4555.9	2.8	0.0005	0.3	>3100
Fe II	4515.3	2.8	0.0007	0.2	>1500
Fe II	4522.6	2.8	0.0017	0.4	>1300
Fe II	4508.3	2.9	0.0009	0.3	>1700
Fe II	5169.0	2.9	0.017	0.8	>200
Fe II	4549.5	2.9	0.001	0.5	>2700
Fe II	5316.6	3.2	0.0002	0.5	>9100
Fe II	5276.0	3.2	0.0013	0.4	>1100
Fe II	5234.6	3.2	0.0008	0.3	>1600
Fe II	5197.6	3.2	0.0011	0.3	>1100
Fe II	3154.2	3.8	0.031	0.5	>180
Fe II	3167.9	3.8	0.0024	0.6	>280
Fe II	3289.4	3.8	0.0034	0.3	>770
Fe II	3135.4	3.9	0.013	0.5	>420
Fe II	3323.1	4.0	0.003	0.4	>1400
Fe II	3162.8	4.2	0.008	0.7	>920
Fe II	3493.5	4.2	0.0059	0.4	>670
Ni II	3514.0	0.2	0.0033	0.5	>1400
Ni II	3769.5	3.1	0.0036	0.1	>280
Ni II	3576.8	3.1	0.0059	0.3	>510
Ni II	4067.0	4.0	0.0015	0.1	>370

Notes. This is a selection of relatively strong and unblended circumstellar lines. For each ion, they are arranged in terms of increasing lower energy level.
[a] Wavelength is listed in air.
[b] The equivalent width is measured from a direct integral of the flux below the continuum. This value is usually dominated by the circumstellar line as may be seen in Figures 1 and 2.
[c] N is the column density of the ion, following Equations (3)–(48) in Spitzer (1978).
[d] The observed Ca lines are much stronger than the best-fit model considering all Ca lines. We conclude that they have a circumstellar contribution, measured from the spectra by subtracting the photospheric Ca component, i.e., the solid magenta line in Figure 2.

disk mass by the total accretion rate and it is only ~1 hr. The gas must be constantly replenished. In addition, no variability was observed in the circumstellar absorption lines by comparing our three separate HIRES and two separate ESI observations, indicating a relatively smooth azimuthal distribution.

There are at least two ways to generate circumstellar gas. (i) Sublimation from the disrupting planetesimals (Rappaport et al. 2012). The planetesimal's surface can be heated to have a high-Z atmosphere and for planetesimals around WD 1145+017, the mass loss would be in a free streaming limit (Vanderburg et al. 2015). This scenario is very similar to the outgassing of a cometary nucleus when it gets close to the Sun (e.g., Keller et al. 1986). However, the thermal speed is only $\sim$ 1 km s^{-1} and it cannot explain the velocity dispersion of 300 km s^{-1}. (ii) Collisions among the planetesimals. If the tidal disruption event resembles the encounter of comet Shoemaker–Levy 9 with Jupiter (Benner & McKinnon 1995), there could exist a stream of disintegrating planetesimals in eccentric orbits with periastrons inside the white dwarf's tidal radius. The observed velocity dispersion might represent different post-collision speeds. This is further supported by the broad and asymmetric circumstellar line profiles.

3.3. Origin of the Infrared Excess

WD 1145+017 belongs to a subgroup of polluted white dwarfs that show a strong infrared excess from a dust disk. However, the dust disk appears to be misaligned with the circumstellar gas and the transiting planetesimals (Vanderburg et al. 2015). Here, we discuss several possibilities.

A puffed-up dust disk. We assume the dust particles at the outer edge $100R_{wd}$ have a vertical speed of 30 km s^{-1}, a small fraction of the observed spread in the radial velocity of the circumstellar gas. The dust can travel to a vertical height of 10 R_{wd}, which is sufficient to produce the infrared excess.

A precessing dust disk. At least one more object (very likely a planet) is required to be present in the system to perturb planetesimals into the white dwarf's tidal radius. If the orbital plane of the planet and the dust disk are not aligned, the planet could induce significant precession of the dust disk. In this case, we would expect the infrared flux to vary gradually.

A previous generation dust disk. The dust disk can be produced by a previous tidal disruption event, possibly associated with the one that also polluted the white dwarf's atmosphere. The lifetime of a dust disk is estimated to be between 10^5 and 10^7 years (e.g., Barber et al. 2012). Jura (2008) suggested that a newly arriving object would have a different orbital inclination and mutual collisions can lead to partial evaporation or even total disruption of the dust disk. This scenario is further supported by the discovery of rapid changes in dust and gas disks around polluted white dwarfs (Wilson et al. 2014; Xu & Jura 2014). WD 1145+017 could be a precursor to such systems.

4. CONCLUSIONS

WD 1145+017 is in a unique stage that has a polluted atmosphere, a dust disk, cool circumstellar gas, and multiple transiting planetesimals. In conclusion:

1. We have detected 11 heavy elements in the photosphere. The composition of the accreted planetesimal is similar to those observed in other polluted white dwarfs. The heavy

elements could either come from a burst of accretion induced by the disintegrating planetesimals, a previous tidal disruption event, or both.
2. We have uniquely detected ∼70 circumstellar absorption lines from 8 ions. The lines have broad asymmetric profiles with velocity dispersion $\sim 300\,\mathrm{km\,s^{-1}}$. The gas lifetime is very short and gas must be constantly replenished, possibly by collisions among the disrupting planetesimals.
3. The infrared excess could come from either a puffed-up dust disk, a precessing dust disk, or a previous generation dust disk.

We thank N. Mahesh for helping with the HIRES observing run. This work has been partly supported by the NSF. The authors wish to recognize and acknowledge the very significant cultural role and reverence that the summit of Mauna Kea has always had within the indigenous Hawaiian community. We are most fortunate to have the opportunity to conduct observations from this mountain.

REFERENCES

Barber, S. D., Patterson, A. J., Kilic, M., et al. 2012, ApJ, 760, 26
Benner, L. A. M., & McKinnon, W. B. 1995, Icar , 118, 155
Croll, B., Dalba, P. A., Vanderburg, A., et al. 2015, ApJ, submitted (arXiv:1510.06434)
Debes, J. H., Kilic, M., Faedi, F., et al. 2012, ApJ, 754, 59
Dickinson, N. J., Barstow, M. A., Welsh, B. Y., et al. 2012, MNRAS, 423, 1397
Dufour, P., Kilic, M., Fontaine, G., et al. 2012, ApJ, 749, 6
Farihi, J., Gänsicke, B. T., Wyatt, M. C., et al. 2012, MNRAS, 424, 464
Friedrich, S., Koester, D., Christlieb, N., Reimers, D., & Wisotzki, L. 2000, A&A, 363, 1040
Gänsicke, B. T., Koester, D., Farihi, J., et al. 2012, MNRAS, 424, 333
Gänsicke, B. T., Marsh, T. R., Southworth, J., & Rebassa-Mansergas, A. 2006, Sci, 314, 1908
Holberg, J. B., Bruhweiler, F. C., & Andersen, J. 1995, ApJ, 443, 753
Jura, M. 2008, AJ, 135, 1785
Jura, M., & Young, E. D. 2014, AREPS, 42, 45
Keller, H. U., Arpigny, C., Barbieri, C., et al. 1986, Natur , 321, 320
Kilic, M., von Hippel, T., Leggett, S. K., & Winget, D. E. 2006, ApJ, 646, 474
Klein, B., Jura, M., Koester, D., Zuckerman, B., & Melis, C. 2010, ApJ, 709, 950
Koester, D. 2009, A&A, 498, 517
Koester, D., Gänsicke, B. T., & Farihi, J. 2014, A&A, 566, A34
Melis, C., Dufour, P., Farihi, J., et al. 2012, ApJL , 751, L4
Melis, C., Jura, M., Albert, L., Klein, B., & Zuckerman, B. 2010, ApJ, 722, 1078
Rappaport, S., Levine, A., Chiang, E., et al. 2012, ApJ, 752, 1
Schmidt, G. D., Szkody, P., Henden, A., et al. 2007, ApJ, 654, 521
Sheinis, A. I., Bolte, M., Epps, H. W., et al. 2002, PASP, 114, 851
Spitzer, L. 1978, Physical Processes in the Interstellar Medium (New York: Wiley-Interscience)
Vanderburg, A., Johnson, J. A., Rappaport, S., et al. 2015, Natur, 526, 546
Veras, D., Leinhardt, Z. M., Eggl, S., & Gänsicke, B. T. 2015, MNRAS, 451, 3453
Vogt, S. S., Allen, S. L., Bigelow, B. C., et al. 1994, Proc. SPIE, 2198, 362
Voss, B., Koester, D., Napiwotzki, R., Christlieb, N., & Reimers, D. 2007, A&A, 470, 1079
Wasson, J. T., & Kallemeyn, G. W. 1988, RSPTA, 325, 535
Wilson, D. J., Gänsicke, B. T., Koester, D., et al. 2014, MNRAS, 445, 1878
Xu, S., & Jura, M. 2014, ApJL, 792, L39
Xu, S., Jura, M., Koester, D., Klein, B., & Zuckerman, B. 2014, ApJ, 783, 79
Zuckerman, B., Koester, D., Reid, I. N., & Hünsch, M. 2003, ApJ, 596, 477
Zuckerman, B., Melis, C., Klein, B., Koester, D., & Jura, M. 2010, ApJ, 722, 725